Journal of Energy Storage 62 (2023) 106912

Contents lists available at ScienceDirect

Journal of Energy Storage

journal homepage: www.elsevier.com/locate/est

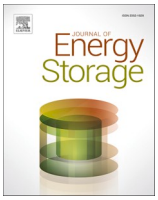

Research papers

Thermal performance of a dynamic insulation-phase change material system and its application in multilayer hollow walls

Zhaoli Zhang [a,*], Nan Zhang [a], Yanping Yuan [a,*], Patrick E. Phelan [b], Shady Attia [c]

[a] School of Mechanical Engineering, Southwest Jiaotong University, Chengdu 610031, China
[b] School for Engineering of Matter, Transport & Energy, Arizona State University, Tempe 85287-6106, United States
[c] Sustainable Building Design Lab, Dept. UEE, Faculty of Applied Sciences, University of Liège, Liège 4000, Belgium

ARTICLE INFO

Keywords:
Phase change material
Building overheating
Dynamic insulation system
Air flow
Thermal resistance

ABSTRACT

The Building integrated with phase change material (PCM) creates a large thermal barrier between indoor thermal environment and ambient, usually resulting in overheating problem in summer. Dynamic insulation system (DIS) based on air flow is introduced into PCM to form a composite structure featured with switchable thermal resistance to address this issue. Theoretical model is built according to phase transition of PCM and heat transfer between PCM and flowing air. Result indicates that thermal resistance can be modified by natural convection and forced turbulence of air. Forced turbulence case obtains the lowest thermal resistance, orderly followed by natural convection and closed cases. Temperature and phase change contour indicate that turbulent air enables to promote uniformity of temperature and phase transition distribution. Larger H/L ratio and height of PCM cavity inducing more intensive air flow are favorable to heat transfer between air and PCM. A DIS-PCM module with low flowing rate or large inputted heat flux produces rapid heat transfer rate and early PCM melting. The Built DIS-PCM module is then coupled with the multilayer hollow wall component to investigate potential application in relieving building overheating issue. Lower average temperature of the interior wall and higher heat dissipation rate from indoor thermal environment verify that the DIS-PCM module enables to resolve building overheating under constant or variable ambient temperature, even at slight temperature difference between indoor and ambient temperatures. Indoor thermal comfortable temperature can be accurately adjusted according to the air flowing rate. In conclusion, the novel DIS-PCM system eliminates building overheating issue through its thermal resistance switch in response to various working scenarios, with substantial benefits to development of latent heat thermal energy storage available to building energy conservation.

1. Introduction

Energy consumed in buildings field has obtained a pivotal position in total global energy consumption [1]. It is increasingly reckoned as the primary source of carbon emission that is responsible for severe environmental issues including global warming, acid rain and smog, etc. [2]. With the continuous promotion of sustainable development, various possible strategies are urgent to be proposed to handle the coupled building energy and environmental problems.

Building energy consumption is mainly focused on heating, cooling, ventilation and lighting, which is dependent on the geographical locations, building types and climates [3,4]. Previous studies proof that energy consumption involved in the building field can be optimized by insulation system, heating, ventilation and air conditioning renovations, and building retrofits, etc. [5]. PCM integrated into a building envelope is identified as a promising method and it generally refers to solid-liquid PCM that possesses advantages of large thermal energy storage density and constant phase transition temperature [6]. It is recognized that PCM is capable of increasing thermal mass of the building envelope, reducing electricity required from HVAC systems and improving building energy efficiency and sustainability. Moreover, PCM utilization in the building envelope can mitigate indoor temperature fluctuation, then achieving stable indoor environment and suitable thermal comfort for occupants.

Zeinelabdein et al. [7] utilized the nocturnal outdoor air as a heat sink via a ventilation process to cool buildings in hot climates. PCM could play an essential role in the effective operation of the free cooling systems by shifting the daytime peak load to the night. Results demonstrated that the temperature difference between the PCM and air at

* Corresponding authors.
E-mail addresses: zzlyzhang@outlook.com (Z. Zhang), ypyuan@swjtu.edu.cn (Y. Yuan).

https://doi.org/10.1016/j.est.2023.106912
Received 3 December 2022; Received in revised form 8 February 2023; Accepted 14 February 2023

appropriate air flow rate would have a significant impact on system performance. Jia et al. [8] designed an effective mean to improve the indoor thermal condition in prefabricated building envelopment by PCM application. Thermal performance and energy consumption of novel prefabricated building were investigated in five different climate regions. Results showed that PCM placed inside the building wall or roof, east or west side building wall is better for energy saving and indoor air temperature improvement. Meng et al. [9] prepared PCM foamed cement with different foaming rate to improve its thermal storage capacity and thermal insulation performance of PCM. Thermal conductivity of the PCM foamed cement was tested under different temperatures and foaming rates. It was found that PCM foamed cement roof performed excellent in reducing internal surface temperature and indoor heat gain, when being placed on the external surface of building roofs. Huang et al. [10] proposed three macro-encapsulated PCM roofs with purpose to weak external heat entering building to reduce air-conditioning energy consumption. Effects of PCM thickness, encapsulation forms, and PCM types on thermal performance of roof systems are analyzed in Moroccan semi-arid and Mediterranean climates. Obtained results could provide guidance for the popularization of PCM roofs in these two climates. Xie et al. [11] discussed the thermal performance evaluation of PCM with thermal conductivity of 0.08 to 49.28 W/(m·°C). A novel index of utilization rate of latent heat (URLH) was proposed to evaluate matching degree between PCM and application background in buildings, and further explore the comprehensive energy-saving effect of PCM under application backgrounds. They found out that PCM had a turning point of about 0.6 W/(m·°C) in thermal conductivity.

Based on aforementioned review, it is concluded that effects of PCM integrated envelopes on thermal performance of buildings have been extensively examined, from both experimental and theoretical perspectives [12]. Technically, PCM can be properly incorporated into various building structures (walls, roofs, ceilings, windows or floors etc.) and work in passive form to improve building thermal performance and energy conservation. Energy saving potential of the PCM integrated envelope is strongly related to numerous factors, such as PCM location, content and thermophysical properties (phase change temperature, latent heat and thermal conductivity, etc.) [13,14]. Prior studies imply that PCM is more effective when incorporated into lightweight construction (wooden wall) over structure having heavy mass (concrete blocks) [15]. Numerous emerging energy saving technologies (PV, solar wall and earth-to-air heat exchanger system, etc.) are extensively introduced into the building field and PCM can be connected with these available technologies to explore synergetic control strategy towards building energy consumption and thermal environment control [16–19]. Building thermal performance can be precisely regulated and improved with rational energy consumption when coupled with PCM [20]. This configuration inevitably creates a large thermal barrier between indoor thermal environment and the exterior wall, which is capable to reduce heat loss to ambient and keep the building thermal insulation. Though effect of ambient temperature swing on building performance is weakened, the indoor overheating problem will become even prominent in hot weather [21]. It has increasingly evolved into one of the tough difficulties existing in passive buildings, especially in PCM integrated envelopes.

Dynamic insulation system (DIS, also called thermal smart materials and systems) is introduced to address the above issue, by means of adjusting apparent thermal resistance of the building envelope according to the climate and indoor conditions to build suitable building thermal environment. On basis of working principles, DIS can be classified into five categories: convection, multilayer, thermal diode, electrochemical regulation and external force field, etc. [22]. Among them, air convection is gradually identified as an efficient approach to be integrated into building envelopes and utilized for energy conservation.

Imbabi [23] firstly simulated performance of a new void space coupled with passive insulation material and active ventilation to deliver low thermal loss and high indoor air quality in buildings with thin wall construction. Built concept could shifted from a passive component to active model to drive the air flow, eliminating the risk of vapor condensation and overheating during extreme summer months. Pflug et al. [24] presented a new translucent element with switchable U-value to prevent the overheating of a well-insulated building. The convection around a translucent insulation panel was controlled by moving this panel vertically within the double glazing unit. An optimized element led to a cooling demand reduction up to 29.6 % of useful energy and large improvement in the summer comfort. Pflug et al. [25] further designed a new switchable window consisting of a series of air-filled cavities that could be rolled up or down between two fixed layers, switching the thermal and optical properties from thermally insulating state to conducting state. The U-value changed from 0.35 W/(m^2·°C) in the insulating state to 2.7 W/(m^2·°C) in the conducting state. Building energy simulation showed that the sum of heating and cooling demands could be reduced by about 30 % with the switchable window application. Koenders et al. [26] investigated performance of a novel type of closed-loop forced convective DIS. Results showed that a ninefold higher U-value was achieved in comparison to insulating state of the system. DIS could reduce the energy consumption and increase the indoor thermal comfort of a typical residential building, under less auxiliary energy than conventional cooling systems. Kishore et al. [22] examined a novel wall design, comprising a PCM layer between two layers of dynamic insulation material. Built wall provided significantly higher energy saving potential than the DIS-only or PCM-only integrated wall and could afford 15–72 % reduction in annual heat gain and 7–38 % reduction in annual heat loss.

Obtainable study reviews testify that DIS can be installed in the wall or window component, with the aim of adjusting thermal resistance based on the building energy demand. The available integration mainly includes two forms: (1) DIS-solar wall to control indoor temperature directly; (2) DIS-multilayer wall or window to regulate indoor temperature indirectly. In brief, the switchable thermal resistance of DIS enables to prevent overheating of a well-insulated building, improving indoor thermal comfort accordingly under less auxiliary energy consumption. However, there are few literatures involved DIS and PCM in multilayer hollow wall system together. There requires a synergistic mechanism between DIS and PCM and phase change heat transfer characteristics of PCM can be substantially affected by DIS. Their transient responds are also responsible to apparent thermal resistance and heat dissipation rate. This paper aims to deal with overheating and energy consumption issue through introduction of DIS-PCM system to the multilayer hollow wall component in a well-insulated building. It is identified that the multilayer hollow wall system has practicable air space for simultaneously loading DIS and PCM. Whereas, PCM has the ability to store extensive thermal energy at almost constant temperature and DIS can promote energy storage of PCM via rationally modification of thermal resistance. The following research initially investigates thermal resistance, heat dissipation performance, temperature variation and phase transition of DIS-PCM system. Detailed configuration of the DIS-PCM-hollow wall system is elaborated and its potential applied in control of building overheating is revealed under specific case condition.

2. Numerical investigation

2.1. Physical model

Various PCM modules are designed in this investigation and two-dimensional schematics of their physical models are illustrated in Fig. 1. It is presented in Fig. 1(a) that a regular multilayer structure is denoted as a closed module (cl case). Amounts of PCM is placed in its middle area. The left and right sides of the PCM layer are filled with air. In order to optimize the heat transfer enhancement of air flowing, an improved PCM module (nc case) equipped with an annular air channel is proposed. The PCM area is reduced, forming two air strips in top and bottom regions of the nc case. Inside air is able to circularly flow under

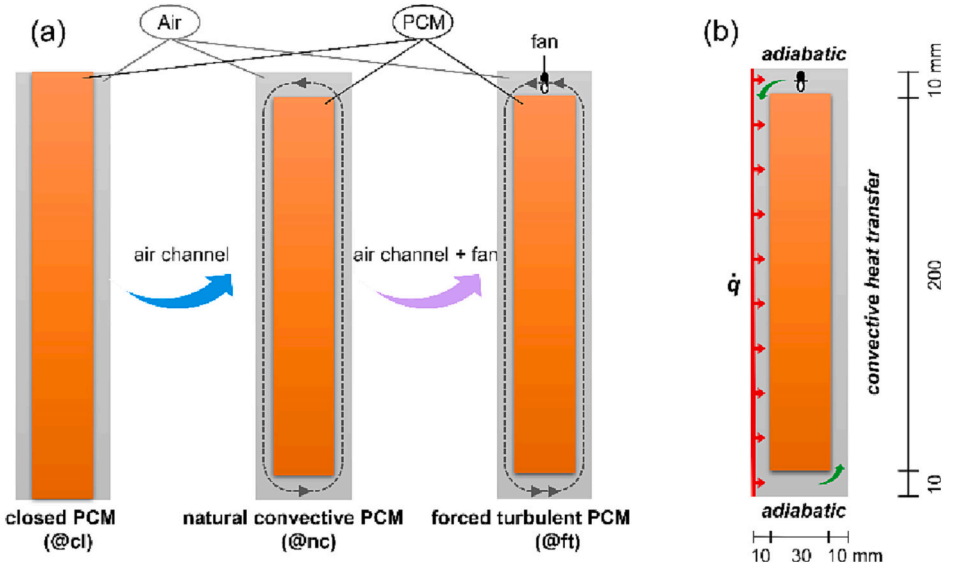

Fig. 1. Physical model of various PCM modules. (a) Configuration of three PCM modules (b) Detailed dimension and boundary condition of the PCM module.

the natural convection motivation derived from thermal buoyancy. Furthermore, a forced turbulent PCM module (ft case, also called the active PCM module) is established through introduction of an electric fan into the nc case, enabling to provide the active driving force for air flow within the annular channel. Theoretically, the electronic fan can not only enhance the air flow magnitude, but also precisely control the air flow according to detailed working environment. Consumed electricity is obtained from excess power at off-peak hours, or green energy including photovoltaic system and thermoelectric generation, etc.

Detailed dimension of PCM modules is indicated in Fig. 1(b) and it is assumed that PCM modules (cl, nc and ft) have specific outside dimension (50 × 220 mm). Left and right intervals between the PCM cavity and module are fixed as 10 mm. Whereas, the width of air channels in top and bottom of nc and ft. cases is placed as 10 mm. The total area of PCM is determined as 6600 mm^2 in cl case and declines to 6000 mm^2 in improved nc and ft. cases. Organic paraffin wax with melting point close to the indoor required temperature is chosen as thermal energy storage medium and Table 1 lists corresponding thermophysical properties [27,28].

2.2. Governing equations

2.2.1. PCM

Paraffin wax acting as excellent thermal energy storage medium will undergo solid-liquid phase transition during the research and several reliable assumptions are established to simplify numerical calculation [29,30].

(1) Liquid PCM belongs to incompressible Newtonian fluid and unsteady laminar flow;

(2) PCM is subjected to thermal buoyancy with the density variation of PCM conforming to the Boussinesq approximation;

(3) Volume change of PCM in solid and liquid is neglected.

Liquid PCM gradually evolves into solid when beings subjected to low temperature and the stored thermal energy can be released to improve the indoor thermal environment. Phase transition between solid and liquid PCM as well as the laminar flow of liquid PCM are believed as tough problems to handle in theoretical simulation. This investigation employs a enthalpy-porosity method to evaluate the phase change heat transfer process, on basis of previous published studies [31,32]. The whole computational domain is treated as a porous zone with the porosity of each cell characterized by liquid fraction (f). The obtained governing equations of PCM in terms of continuity, momentum and energy conservation are separately shown in Eqs. (1)–(3).

$$\frac{\partial(\rho_f)}{\partial\tau}+\nabla\left(\rho_f\vec{u}\right)=0 \tag{1}$$

$$\frac{\partial(\rho_f\vec{u})}{\partial\tau}+\nabla\left(\rho_f\vec{u}\vec{u}\right)=-\nabla p+\mu_f\nabla^2u+\rho_f g\beta_f\left(T_f-T_s\right)+S_{u,f} \tag{2}$$

$$\frac{\partial(\rho_f H)}{\partial\tau}+\nabla\left(\rho_f\vec{u}H\right)=\nabla\left(\lambda_f\nabla T\right)+S_{r,f} \tag{3}$$

where τ is the time; $\vec{u}$ is the velocity vector of liquid PCM; ρ_f, μ_f, λ_f, p and β_f denote the density, dynamic viscosity, thermal conductivity, pressure and thermal expansion coefficient of PCM; $S_{u,f}$ and $S_{r,f}$ are the source terms in momentum and energy conservation equations, $S_{u,f}=-uA_{mushy}\frac{(1-f)^2}{f^3+\varnothing}$, $A_{mushy}=10^5$, $\varnothing=0.001$; H presents the PCM enthalpy that is normally equal to the sum of sensible heat (H_s) and latent heat (L).

$$H=H_s+fL \tag{4}$$

$$H_s=H_{ref}+\int_{T_{ref}}^{T}c_p dT \tag{5}$$

where H_{ref} and T_{ref} mean the reference enthalpy and temperature. The liquid fraction(f) is used to indicate the volume proportion of melted PCM during the research. f will linearly change within the scope of 0 and

Table 1
Thermophysical properties of utilized PCM and air.

Properties	PCM		Air (K)
	Solid	Liquid	
ρ(kg/m^3)	950	920	2935.38525/RT
c_p(J/(kg·°C))	2050	2250	1047.63657–0.372589265 T + 9.45304214 × 10^{-4} T^2–6.02409443 × 10^{-7} T^3 + 1.2858961 × 10^{-10} T^4
κ(W/(m·°C))	0.27	0.20	−0.00227583562 + 1.15480022 × 10^{-4} T-7.90252856 × 10^{-8} T^2 + 4.11702505 × 10^{-11} T^3–7.43864331 × 10^{-15} T^4
μ(Pa·s)	–	0.0032	0.6 × (−8.38278 × 10^{-7} + 8.35717342 × 10^{-8} T-7.69429583 × 10^{-11} T^2 + 4.6437266 × 10^{-14} T^3–1.06585607 × 10^{-17} T^4)
L(kJ/kg)	198		
T_m(°C)	25.5	30.5	
β(1/K)		0.0006	-(1/ρ)*(dρ/dt)

1 for PCM in the mushy region between solid and liquid. $f = 0$ or 1 represents PCM is in solid or liquid state.

$$f = \begin{cases} 0, T_f < T_s \\ \dfrac{T_f - T_s}{T_l - T_s}, T_s < T_f < T_l \\ 1, T_f > T_l \end{cases} \quad (6)$$

where T_s and T_l are the initial and terminal temperatures of PCM melting zone.

2.2.2. Air

It is identified that air can be divided into two groups according to its flow condition in the DIS-PCM module. The first group is the air flowing through the promotion of thermal buoyancy as indicated in cl and nc cases of Fig. 1(a). Whereas, the second group belongs to the air circulating under the driving force of an electric fan. Since the flow state and working principle are different, this paper intends to discuss them separately in the following research.

(1) Air in natural convection

Air is believed as working under laminar flow in cl and nc cases where no additional force is exerted and the correspondent governing equations are listed as follows [33,34].

$$\frac{\partial(\rho_a)}{\partial\tau} + \nabla(\rho_a \vec{u}) = 0 \quad (7)$$

$$\frac{\partial(\rho_a \vec{u})}{\partial\tau} + \nabla(\rho_a \vec{u}\vec{u}) = -\nabla p + \mu_a \nabla^2 u + \rho_a g \beta_a (T_a - T_{ref}) \quad (8)$$

$$\frac{\partial(\rho_a c_{p,a} T)}{\partial\tau} + \nabla(\rho_a c_{p,a} \vec{u} T) = \nabla(\lambda_a \nabla T) + S_{r,ac} \quad (9)$$

where τ is the time; $\vec{u}$, ρ_a, $c_{p,a}$, μ_a, λ_a, p and β_a denote the velocity vector, density, specific heat, dynamic viscosity, thermal conductivity and pressure of air; $S_{r,ac}$ presents the source term in energy conservation equation for natural convection heat transfer between air and PCM.

(2) Air in forced convection

On account of heat transfer efficiency in forced convection is greater than that in natural convection, air circulation in the annular channel of ft. case largely enhance the heat transfer rate between air and PCM [35,36]. The forced convection of air is regarded as low Re k-ε turbulent flow with related governing equations listed as follows:

$$\frac{\partial(\rho_a)}{\partial\tau} + \nabla(\rho_a \vec{u}) = 0 \quad (10)$$

$$\frac{\partial(\rho_a k)}{\partial t} + \rho_a \vec{u} \bullet \nabla k = \nabla \bullet \left[\left(\mu_a + \frac{\mu_t}{\sigma_k} \right) \nabla k \right] + P_k - \rho\varepsilon \quad (11)$$

$$\frac{\partial(\rho_a \varepsilon)}{\partial t} + \rho_a \vec{u} \bullet \nabla \varepsilon = \nabla \bullet \left[\left(\mu_a + \frac{\mu_t}{\sigma_\varepsilon} \right) \nabla \varepsilon \right] + C_{1\varepsilon} \frac{\varepsilon}{k} P_k - f_\varepsilon C_{2\varepsilon} \rho \frac{\varepsilon^2}{k} \quad (12)$$

$$\frac{\partial(\rho_a c_{p,a} T)}{\partial\tau} + \nabla(\rho_a c_{p,a} \vec{u} T) = \nabla(\lambda_a \nabla T) + S_{r,af} \quad (13)$$

where k is turbulent kinetic energy, $k = \frac{\overline{u_i' u_i'}}{2}$; ε is turbulent dissipation rate, $\varepsilon = \frac{\mu}{\rho} \overline{\left(\frac{\partial u_i'}{\partial x_k}\right)\left(\frac{\partial u_i'}{\partial x_k}\right)}$; μ_t is turbulent viscosity, $\mu_t = \rho f_\mu C_\mu \frac{k^2}{\varepsilon}$; P_k is the production term, $P_k = \mu_t(\nabla \vec{u} : (\nabla \vec{u} + (\nabla \vec{u}^t)) - \frac{2}{3}(\nabla \bullet \vec{u})^2) - \frac{2}{3}\rho_a k \nabla \bullet \vec{u}$; other constants, $C_{1\varepsilon} = 1.5$, $C_{2\varepsilon} = 1.9$, $C_\mu = 0.09$, $\sigma_k = 1.4$ and $\sigma_\varepsilon = 1.4$; $S_{r,af}$ presents the source term in energy conservation equation for forced convection heat transfer between air and PCM.

2.3. Initial and boundary conditions

2.3.1. Initial condition

All PCM is assumed as solid with initial temperature of 20 °C prior to investigation. The air has identical initial temperature to that of PCM. Initial velocities of air and PCM are 0 in the monument conservation equation.

2.3.2. Boundary conditions

It is supposed that PCM modules are well sealed by insulated material in their top and bottom surfaces, producing adiabatic condition towards these boundaries. The left boundary is subjected to constant heat flux of 50 W/m^2 and the right surface is presumed as convective heat transfer with heat transfer coefficient and temperature of 5.5 W/(m^2·°C) and 32 °C, respectively. Both the air and liquid PCM can flow within the PCM module during melting process and pressure zero point needs to be arranged in the corners of air and PCM cavities due to the closed circulation. It is also seen in Fig. 1(b) that an electric fan installed in the ft. case has flow rate of 0.5 m/s during the investigation.

2.4. Model solving, independence and validation

2.4.1. Model solving

The finite element method embedded in COMSOL Multiphysics is utilized to solve governing equations of continuity, momentum and energy conservation that are discretized through staggered grid technology within the computational region. The free step backward differentiation formula controls calculation time steps within a rational order and a parallel direct solver with a rational residual error is about to solve the residual equations. Relative residual of 10^{-5} is converged for continuity, momentum and energy conservation equation at each time step of the numerical calculation in order to maintain a highly accurate resolution.

2.4.2. Independence

The unstructured grid consisting of triangular element is adopted in this calculation, on account of COMSOL has its inherent capacity to implement adaptive remeshing. Mesh number is of crucial importance to the finite element method. Its independency is thus discussed in detail before conducting the numerical investigation. Five mesh numbers of 7962, 11,230, 29,580, 48,450 and 65,720 are checked in its independency with the results plotted in Fig. 2. Average temperature and heat dissipation rate on right surface of ft. PCM case as function of measured time under heat flux of 50 W/m^2 is shown in Fig. 2. It is perceived in Fig. 2 that the transient temperature and heat dissipation rate are nearly

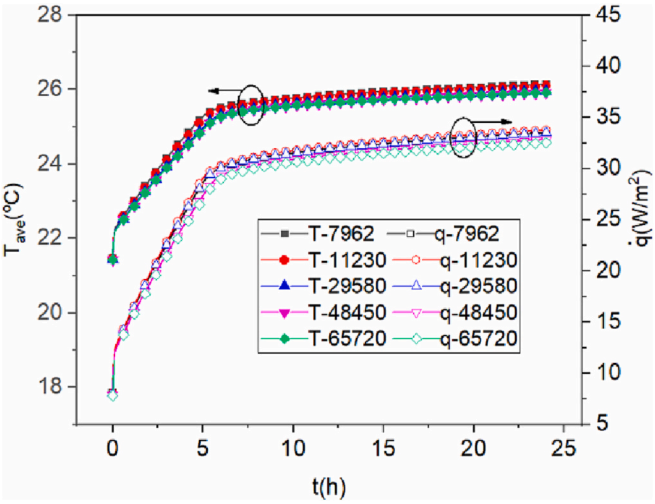

Fig. 2. Mesh independence of built numerical model.

overlapped when the mesh number is larger than 48,450. The results almost maintain constant with continuous augment of mesh number. Whereas, the corresponding calculated process will take much longer time under the condition of larger mesh number. Therefore, the mesh number of 48,450 is recommended in the following research, taking computational accuracy and saving costs into consideration.

2.4.3. Validation

Validation of built mathematical model is accomplished by means of comparison between experimental and simulated results under identical condition. Constant heat flux of $\dot{q} = 4410\ W/m^2$ is exerted in the corresponding experiment. Paraffin wax (melting peak temperature of 45.8 °C, latent heat of 197 kJ/kg) is employed as PCM utilized in the melting process. It is indicated in Fig. 3 that temperatures of PCM (T_2, T_5 and T_8) obtained from built numerical model are in excellent accordance with experimental results of phase change unit with the elapse of time. It can be implied from the comparable results that built theoretical model is accurate enough to be utilized in the next study.

3. Results and discussion

3.1. Thermal performance of DIS-PCM system

3.1.1. Heat dissipation rate and thermal resistance

Temperature on the right surface is higher than left which leads to apparent heat dissipation from right to left side. Average heat dissipation rate of the PCM module calculated from Eq. (14) is elaborated in Fig. 4. It is detected that all of them increase generally with the elapse of time. These sights are largely attributed to air and PCM flow, enhancing heat transfer performance between them. Fig. 4(a) displays that average heat dissipation rate of the PCM module ascends obviously in the initial stage. The turning points appear at roughly 2.5, 3.1 and 4.4 h and PCM modules present slow increasing in average heat dissipation rate since then. Thermal energy is mainly stored in PCM modules in the form of latent heat at this point. With the elapse of time, the average heat dissipation rate of cl case can reach up to merely 16.119 W/m^2 at 24 h. Whereas, natural convection and forced turbulent flow of airs are capable of improving average heat dissipation rate and the final maximal result approaches to 28.387 and 34.192 W/m^2 with regard to nc and ft. cases, respectively.

$$\overline{\dot{q}_{dis}} = \frac{\int \dot{q}_{dis} dh}{H} \tag{14}$$

where $\dot{q}_{dis}$ represents transient heat dissipation rate from the right boundary; H is height of the PCM module.

$$R = \frac{T_0 - T_i}{\dot{q}_{in}} \tag{15}$$

where T_0 and T_i denote the transient temperatures of top, middle and bottom points at left boundary and corresponding points at the right boundary of various PCM modules; $\dot{q}_{in}$ is the inputted heat flux at the left boundary.

Thermal resistance (Eq. (15)) can be significantly modified by natural convection and forced turbulent flow of airs. This research selects three positions (top, middle and bottom) as sampling points shown in Fig. 4(b). The calculated thermal resistance is exhibited in Fig. 4(c)–(e) and it is found that transient thermal resistance of cl case is larger than those of nc and ft. cases at top points. The PCM module obtain thermal resistance of approximately 0.62, 0.43 and 0.21 K/W in cases of cl, nc and ft. at 24 h. At middle points, the nc and ft. PCM cases show remarkable improvement to thermal resistance owing to air flow. Air convection is beneficial to heat transfer from left to right side of the PCM modules. Considering air flowing of forced convection is more intense than that of natural convection, the cl case gains largest thermal resistance, followed by nc and ft. PCM cases. It is determined that thermal resistance of the cl case at 24 h is 0.47 K/W, which is far larger than those of nc and ft. cases (0.32 and 0.14 K/W). Fig. 4(e) indicates that natural convection of air causes bottom points in nc case to possess the lowest thermal resistance, compared to ft. and cl cases. This is attributed to the nonuniformity of air temperature. Thermal buoyancy exceeds the forced convection at bottom position, indicating improved heat transfer and reduced thermal resistance. The average thermal resistances are approximately 0.31, 0.19 and 0.29 K/W in terms of cl, nc and ft. cases.

3.1.2. Temperature contour and right boundary temperature

Temperature contour of the PCM module is described in Fig. 5 and it is observed in Fig. 5(a) that the temperatures on the left surface are larger as result of directly contacting with heat source. Air natural convection results from thermal buoyancy, producing upward air flow along the PCM module. The air domain is closed in cl case, while that in nc case is an annular channel. Thermal energy can be dissipated rapidly to the right boundary in nc case, forming higher air temperature contour in the left part of cl case and lower air temperature contour in left part of nc case. Provided that forced turbulent is adopted in ft. case, air flows much faster and its air temperature tends to be more uniformed than that in nc case. Therefore, only slight temperature fluctuation is observed along the height of left part in ft. case. Fig. 5(a) also indicates that high temperature contour is found in the upper region of PCM cavity in cl and nc cases. This phenomenon is contributed to high-temperature air floats up along the PCM modules driven by the thermal buoyancy. Intensive heat transfer between air and PCM leads to PCM with high temperature in the upper region. Low air temperature of the ft. case weakens the heat transfer between air and PCM, producing low temperature contour in related PCM domain.

Temperature profiles of three points at right boundary of the PCM module are exhibited in Fig. 5(b)–(d) and it is found that transient temperatures of them all increase with the elapse of time. The nc case possesses the maximal temperature at the top point compared to other

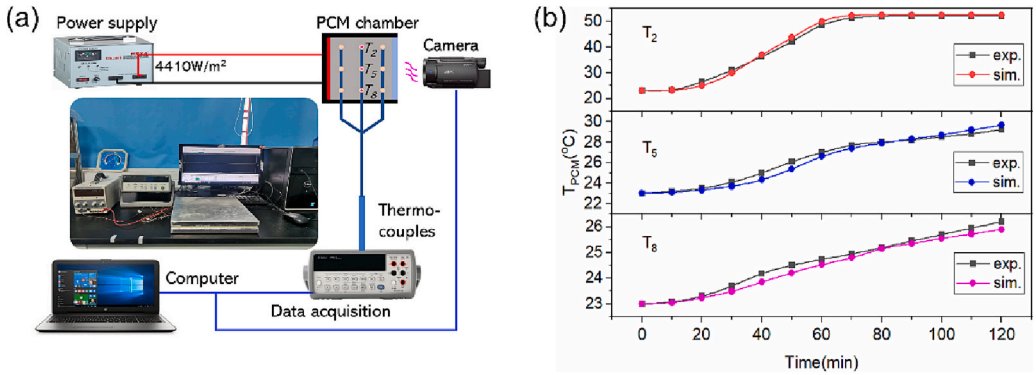

Fig. 3. Validation of the built numerical model. (a) Experimental diagram; (b) PCM temperature.

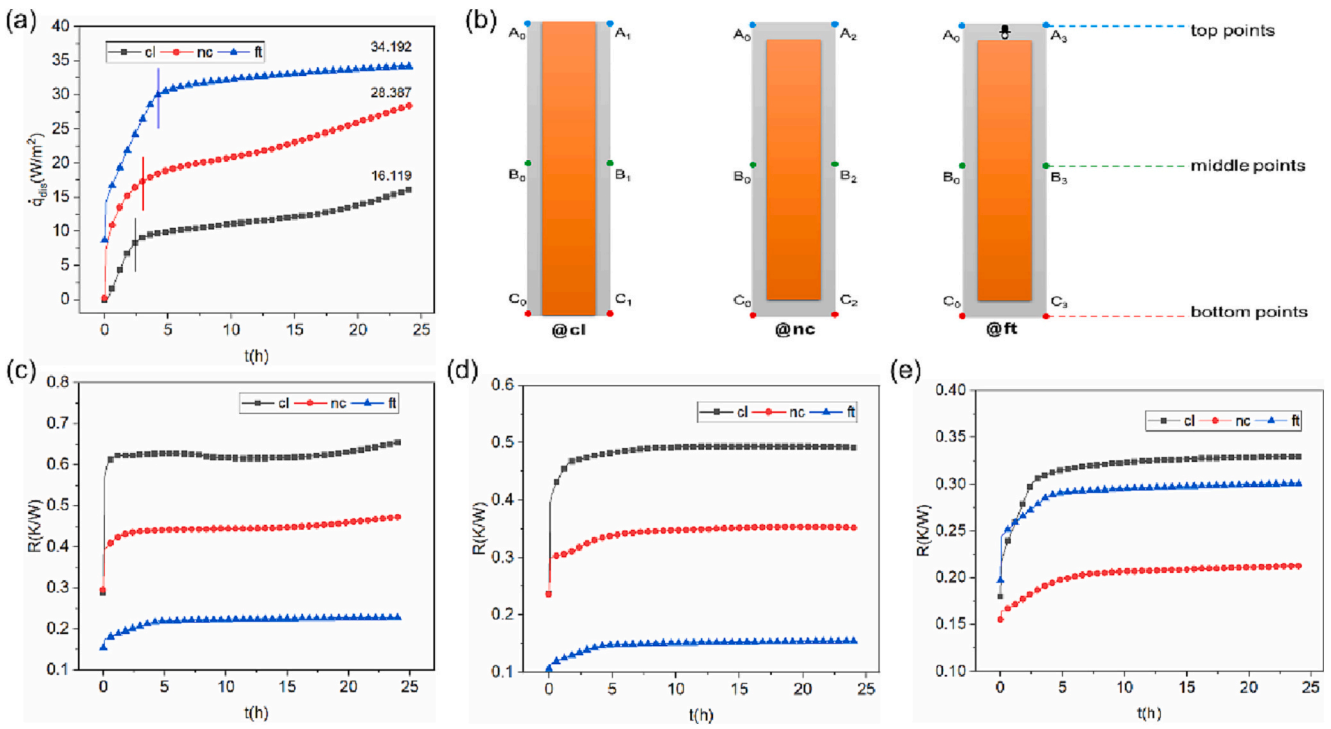

Fig. 4. Effective heat dissipation rate and thermal resistance of DIS-PCM system (u_{air} = 0.5 m/s, $\dot{q}$=50 W/m^2). (a) Heat dissipation rate; (b) Sample points; (c) Thermal resistance at top points (A1-A3); (d) Thermal resistance at middle points (B1-B3) and (e) Thermal resistance at bottom points (C1-C3).

two cases, owing to the high-temperature air subjected to upward thermal buoyancy. The biggest temperature difference is determined as 8.88 °C between nc and ft. cases. The ft. case employs forced air turbulence that enables to show great heat dissipation rate to right boundary and uniformed air temperature within the air domain. Middle point is found to obtain the largest transient temperature in ft. case, followed by nc and ft. cases. Temperature difference can reach up to approximately 3.76 °C between ft. and cl cases. Additionally, thermal buoyancy induces low temperature air to accumulate at bottom of the PCM module. The sampling point of nc case thus has the least temperature in comparison to cl and ft. cases, as indicated in Fig. 5 (d). The maximal temperature difference between ft. and nc cases is calculated as 4.35 °C at 24 h.

3.1.3. Phase change contour and liquid fraction of PCM

Transient phase transition of PCM in three modules is evaluated and phase change contours at specific measured points of time are depicted in Fig. 6. It is released in Fig. 6 (a) that PCM encapsulated in cl case starts to melt from the left of PCM region due to the heat source installed on the left boundary. Natural convection of liquid PCM under the thermal buoyancy further accelerates the PCM melting on top part of the PCM cavity. Thermal energy will be accumulated in the left-top region of PCM modules, with obvious color change in phase change contour. In view of nc case, natural convection of air will be preformed within the annular air channel, bringing more thermal energy dissipated from the right boundary compared to cl case. Therefore, the melting rate of PCM becomes slowly and phase change contour tends to level change shifting from top to bottom of the PCM module. The ft. case gains more slight variation to phase change contour than that of cl or nc case at the same testing point of time, mainly resulting from forced turbulence of air confined in the air channel. The related heat dissipation rate of ft. case on the right boundary is also largest as found in Fig. 4.

Fig. 6 (b) presents transient liquid fraction of PCM changed with measured time in various PCM modules. It is perceived that PCM in ft. case needs longer time to start to melt over cl and nc cases, as more thermal energy can be dissipated from the right boundary under air forced turbulence. Similarly, air natural convection inside the annular channel enables to promote the heat dissipation performance. PCM then melts slower in nc case, arising lower liquid fraction of PCM compared to the cl case. Liquid fraction of PCM encapsulated in three modules attains remarkable increase with argument of time. It is obtained that the liquid fraction of PCM in cl case ascends to approximately 0.518 at 24 h. Whereas, it decreases The nc and ft. cases gain maximal results of merely 0.424 and 0.218 in terms of liquid fraction of PCM.

3.2. Parametric analysis of DIS-PCM system

The Above study testifies that ft. case demonstrates noticeable heat dissipation performance and uniformed PCM melting in contrast to cl and ft. cases, implying extensive application potential in thermal management. This paper thus employs ft. case as the DIS-PCM system analyzed in the following study. Four critical parameters, including H/L ratio and height of PCM cavity, air flowing rate and inputted heat flux, are selected and their effects on thermal performance of the DIS-PCM system are discussed in detail.

3.2.1. H/L ratio of PCM cavity

PCM is properly packaged in the ft. case with air flowing in forced turbulence. Theoretically, larger height to length (H/L) ratio of PCM cavity induces more intensive air natural convection, which is favorable to heat transfer between air and PCM. Various H/L ratios of PCM cavity with identical area (6000 mm^2) are configured in Fig. 7. It is illustrated in Fig. 7(a) that four PCM configurations placed in this investigation are denoted as H160 (160 × 37.5 mm), H180 (180 × 33.333 mm), H200 (200 × 30 mm) and H210 (210 × 28.571 mm), respectively. Effect of H/L ratio on liquid fraction of PCM in ft. case is displayed in Fig. 7(b). Given that air takes time to reach the melting point of PCM, it is observed that PCM is maintained in the solid during the initial stage. The solid period lasts approximately 5.6, 4.9, 3.3 and 2.5 h for H160, H180, H200 and H210 cases. From then on, the liquid fraction increases linearly as the measured time rises. The H/L ratio of PCM cavity leads to a large air-PCM contacting area, generating rapid convection heat transfer

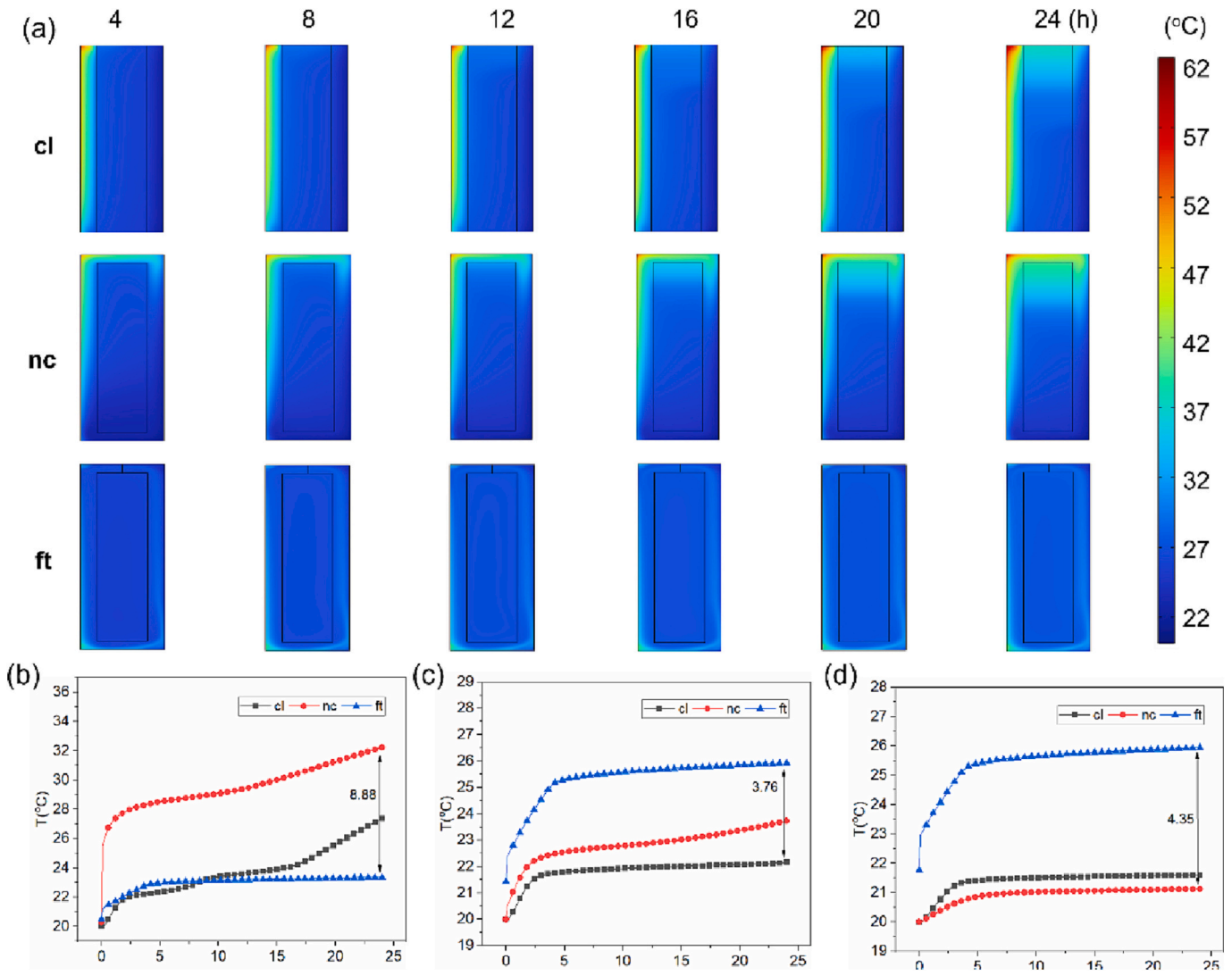

Fig. 5. Temperature contour and temperature profile of sample points at right boundary of the PCM module (u_{air} = 0.5 m/s, $\dot{q}$=50 W/m^2). (a) Temperature contour; (b) Temperature profile at top point; (c) Temperature profile at middle point and (d) Temperature profile at bottom point.

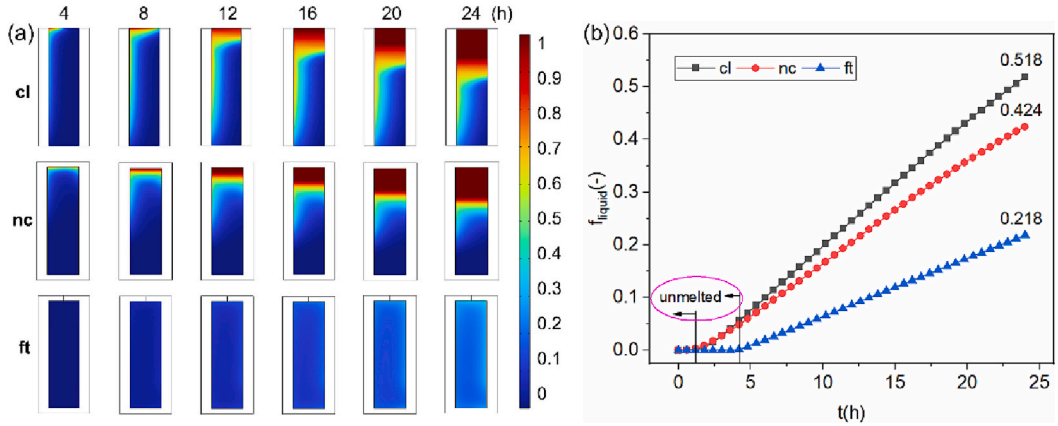

Fig. 6. Phase change contour and liquid fraction of PCM in modules (u_{air} = 0.5 m/s, $\dot{q}$=50 W/m^2). (a) Phase change contour and (b) Liquid fraction.

between them. The growth rate of liquid fraction in H210 case is largest, followed by H200, H180 and H160 cases orderly. When the measured time reaches at 24 h, the maximal result respectively climbs up to 0.252, 0.218, 0.160 and 0.139 in the cases of H210, H200, H180 and H160, indicating solid PCM unable to be fully melted.

Fig. 7(c) exhibits the effects of H/L ratio on heat dissipation rate of the ft. case and it is significant that heat dissipation rate in each case firstly increases with the augment of measured time. The increasing rate

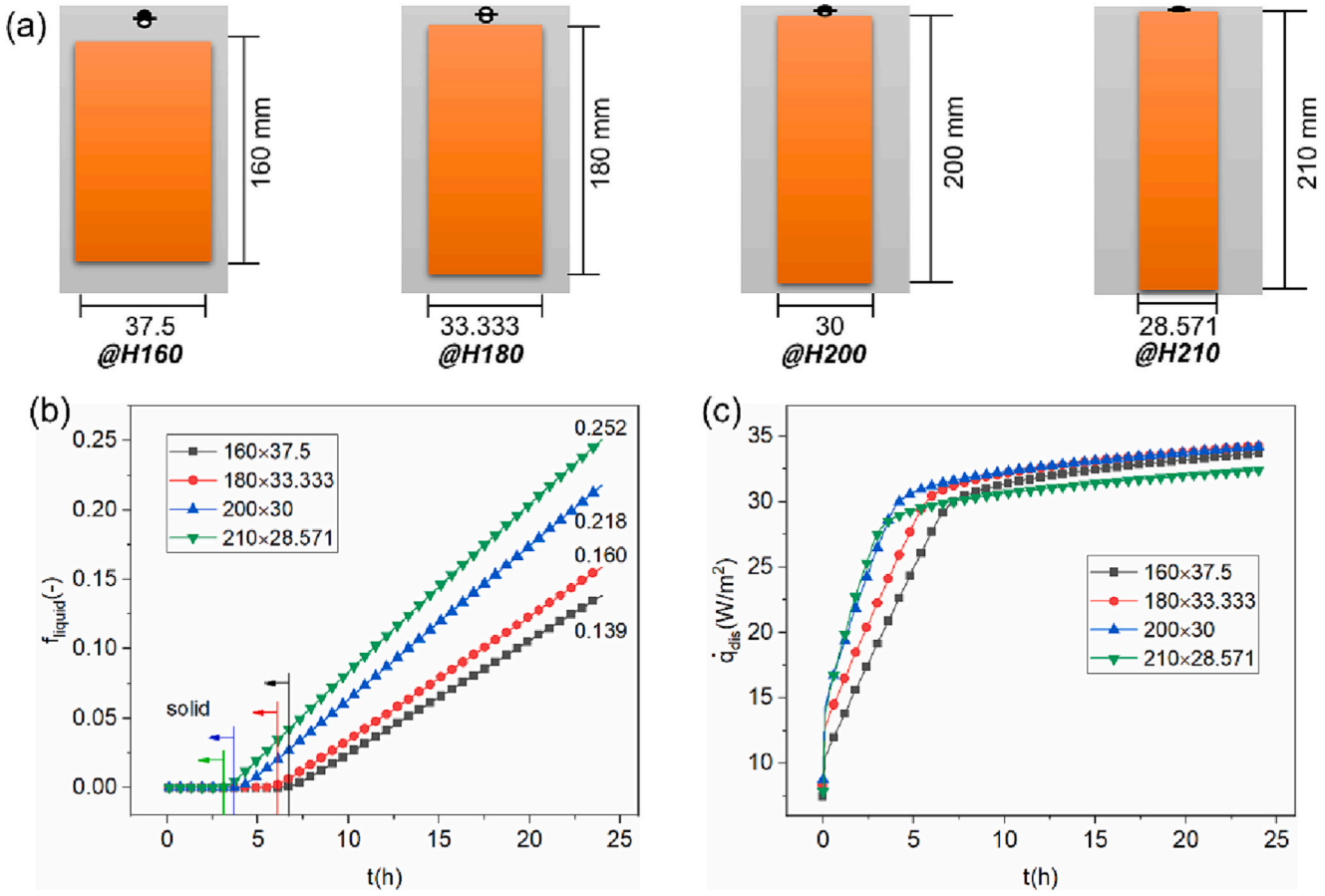

Fig. 7. Effect of H/L ratio on ft. case performance (u_{air} = 0.5 m/s, $\dot{q}$=50 W/m^2). (a) Configuration; (b) Liquid fraction of PCM and (c) Heat dissipation rate.

is also enlarged as the height of PCM cavity ranges from 160 to 210 mm, which is due to improved natural convection and air-PCM contacting area. With the continuous elapse of time, Heat dissipation rate of the ft. case basically reach stable results. More thermal energy is utilized to melt PCM rather than dissipating from the right boundary, presenting lower heat dissipation rate in H210 case contrast to the other cases. The heat dissipation rate of ft. case fluctuates between 32.399 and 34.237 W/m^2 at 24 h.

3.2.2. *Height of PCM cavity*

The ft. cases having various PCM cavity heights are designed in Fig. 8 (a) and it is obtained that ft. cases are separated into four configurations: H100 (100 mm), H200 (200 mm), H600 (600 mm) and H1000 (1000 mm). Whereas, the width of ft. case is maintained as constant of 30 mm in the investigation. Larger height of ft. case causes longer effective contacting time, which is conducive to improve heat transfer performance between air and PCM. The ft. case with larger height contains more PCM and melt earlier under identical heat flow rate. Liquid fraction of PCM increases with the augment of PCM cavity height. Specifically, the liquid fraction of PCM is determined as 0.154 for H100 at 24 h. It will orderly ascend to 0.218, 0.265 and 0.290 when experiments of H200, H600 and H1000 cases last for 24 h. Effects of PCM cavity height on heat dissipation rate are depicted in Fig. 8(c) and it is presented that heat dissipation rate increases dramatically as the measured time elapses in any ft. case. Heat dissipation rate is discovered to initially increase with the PCM cavity height rising from 100 to 200 mm, and then shift to decrease with the PCM cavity height rising from 200 to 1000 mm, as the measured time elapses. The heat dissipation rates of H100-H1000 cases at 24 h are calculated up to 33.523, 34.192, 32.4 and 30.551 W/m^2, respectively.

3.2.3. *Air flowing rate*

Air flowing rate is a crucial factor to performance of ft. case and Fig. 9 illustrates detailed effects of flowing rate on the ft. case performance. It is released that air flowing enables to boost PCM melting in the cavity and liquid faction of PCM incorporated in ft. case increases remarkedly with the augment of measured time. Lower flowing rate of air results in faster heat transfer rate between air and PCM, which then produces earlier melting in contrast to the ft. case with higher flowing rate. More specifically, the lower the flowing rate, the faster heat transfer rate between air and PCM and the earlier melting of PCM in ft. case. It is demonstrated in Fig. 9(a) that liquid fraction of PCM decreases substantially as the flowing rate rising from 0.05 to 1.00 m/s. The liquid fraction of PCM at measured time of 24 h is found as 0.417 for ft. case with 0.05 m/s, then declining to approximately 0.325, 0.218, 0.173 and 0.126 under higher velocity of 0.10–1.00 m/s. Fig. 9(b) further describes the heat dissipation rate from right boundary of the ft. case and it is achieved that heat dissipation rate increases with the augment of measured time. High air flowing rate contributes to larger heat dissipation rate. The maximal heat dissipation rate of 23.837 W/m^2 appears at ft. case containing air flowing rate of 0.05 m/s. Related maximal heat dissipation rate separately increases to 29.368, 32.869, 33.911, 34.192 and 34.073 W/m^2, with air flowing rate of 0.10, 0.25, 0.50, 0.75 and 1.00 m/s.

3.2.4. *Inputted heat flux*

Thermal performance of ft. case can be substantially changed by the inputted heat flux. Five heat fluxes are included in this investigation and their effects on performance of ft. cases are elaborated in Fig. 10. Increasing inputted heat flux is beneficial to thermal energy stored in PCM cavity and heat dissipation rate. The melting start time is observed to be sharply shorten by large inputted heat flux, while liquid fraction of

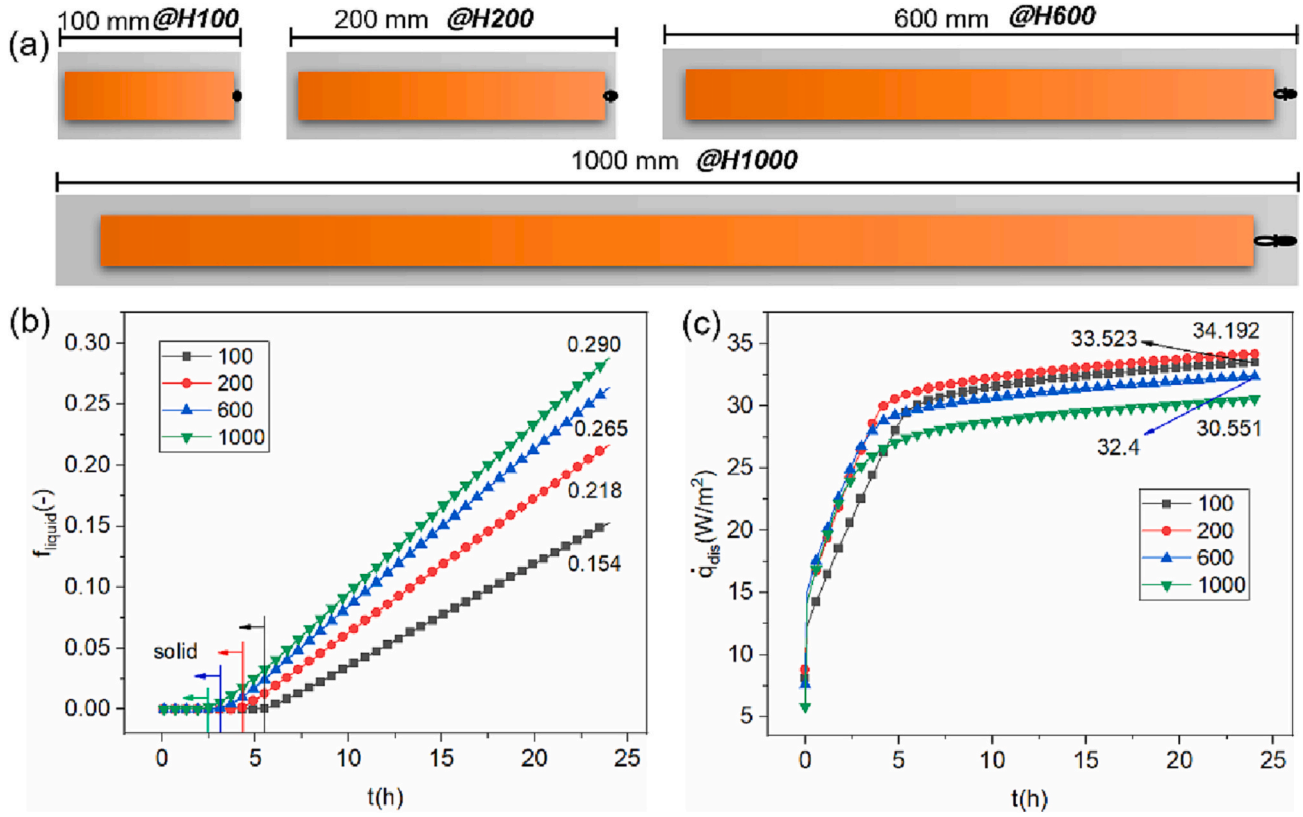

Fig. 8. Effect of PCM cavity height on ft. case performance (u_{air} = 0.5 m/s, $\dot{q}$=50 W/m^2). (a) Configuration; (b) Liquid fraction of PCM and (c) Heat dissipation rate.

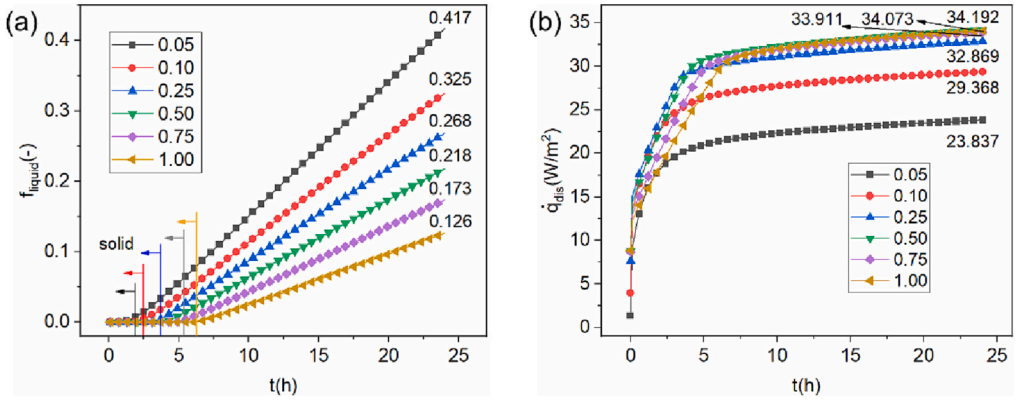

Fig. 9. Effect of air flowing rate on ft. case performance ($\dot{q}$=50 W/m^2). (a) Liquid fraction of PCM and (b) Heat dissipation rate.

PCM increases rapidly with the augment of inputted heat flux. It is calculated that liquid fraction of PCM can rise up to 0.827 for the ft. case subjected to heat flux of 125 W/m^2 at 24 h, in comparison to merely 0.616, 0.413, 0.218 and 0.037 for inputted heat flux of ft. cases declining to 100, 75, 50 and 25 W/m^2. Fig. 10(b) reveals transient heat dissipation rate varied with inputted heat flux. It is considered that more thermal energy can be stored in the PCM under larger heat flux. Heat dissipation rate of the ft. case increases noticeably as measured time rises, arriving the stable stage earlier under higher heat flux. Afterwards, the heat dissipation rates of ft. cases at 24 h slightly increase to 24.798, 34.192, 42.815, 51.174 and 61.462 W/m^2 for inputted heat flux of 25, 50, 75, 100 and 125 W/m^2, respectively.

3.3. Application in multilayer hollow walls

Based on the aforementioned discussion, it is concluded that built PCM modules have the incomparable capability to reduce thermal resistance and accelerate heat dissipation. To solve building overheating problem and create suitable indoor thermal environment, three PCM modules including cl, nc and ft. cases are integrated into the multilayer hollow wall systems with detailed configurations illustrated in Fig. 11. Several metal rods are fixed on the front and back surfaces in order to support the PCM modules. Thus, structural performance of the built wall components can be rationally inferred as robust.

The partial multilayer wall system is designed with related dimension fixed as 330 mm in width and 600 mm in height. The multilayer wall system consists of four layers: 20 mm exterior wallboard, 240 mm brick, 50 mm PCM module and 20 mm interior layer. Their thermophysical properties are listed in Table 2. Two working scenarios including constant and variable ambient temperatures are individually considered in the following research. Average temperature on the exterior or interior wall of a multilayer wall system can be determined

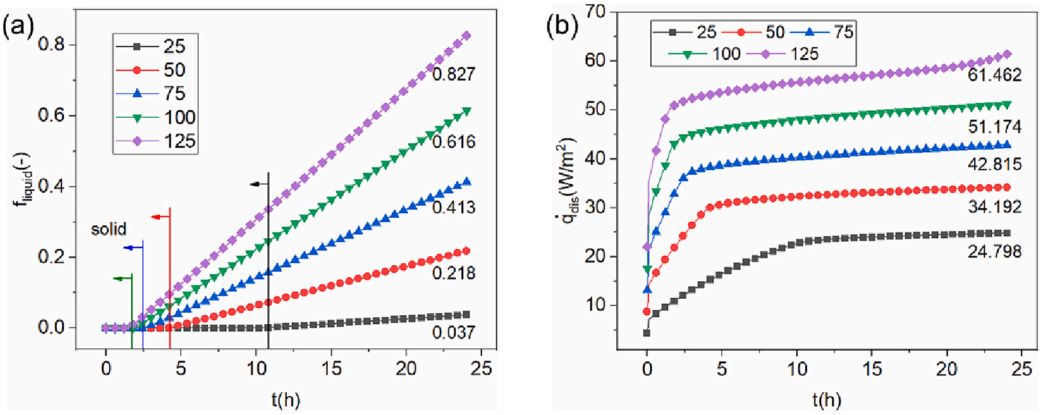

Fig. 10. Effect of inputted heat flux on ft. case performance (u_{air} = 0.5 m/s). (a) Liquid fraction of PCM and (b) Heat dissipation rate.

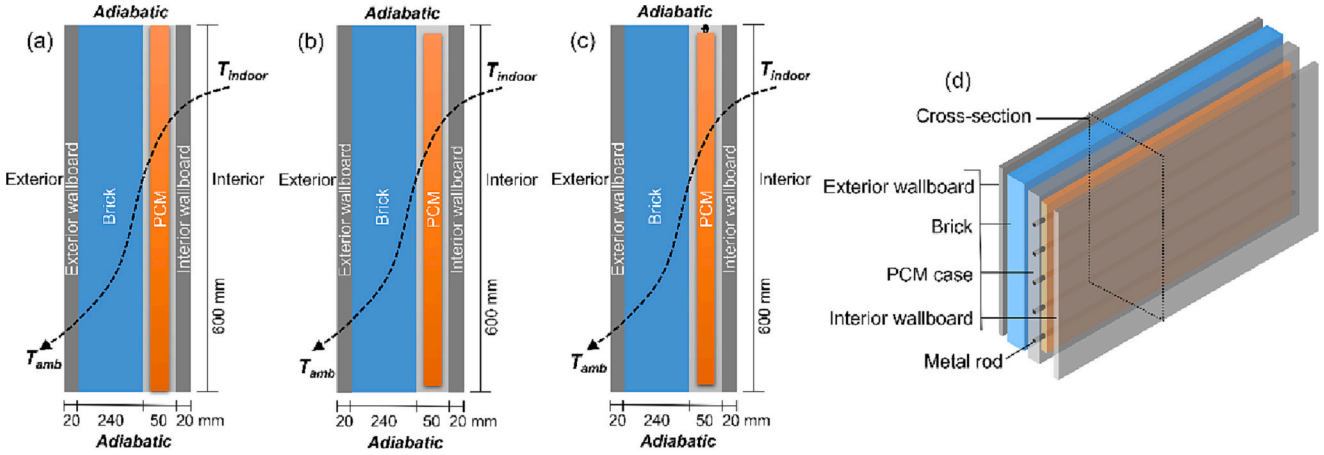

Fig. 11. Schematic of multilayer hollow wall components with various PCM modules. (a) 2D section of the wall with cl PCM case; (b) 2D section of the wall with nc PCM case; (c) 2D section of the wall with ft. PCM case and (d) 3D structure of the wall.

Table 2
Thermophysical properties of utilized wallboard and brick.

Properties	Wallboard	Brick
ρ(kg/m^3)	1922	1200
c_p(J/kg·°C)	837.4	795.5
κ(W/(m·°C))	1.12	0.75

through the Eq. (16).

$$\overline{T} = \frac{\int \dot{T} dh}{H} \tag{16}$$

where T denotes transient temperature on the exterior or interior wall; H is height of the multilayer wall system.

3.3.1. Constant ambient temperature

Thermal performance of the multilayer wall system is analyzed based on the initial temperature of 20 °C. The ambient and indoor temperatures are individually fixed at 20 and 32 °C. It is elaborated in Fig. 11 that the other surfaces including top and bottom are believed as adiabatic. Fig. 12 exhibits related theoretical calculation result of the built multilayer wall system at constant ambient temperature. It is significant that average temperature of the interior wall increases noticeably with the augment of measured time. This sight is ascribed to thermal energy continuously transferred from indoor thermal environment to the interior wall. The nc and ft. cases have lower thermal resistance and larger heat dissipation rate compared to cl case. Average temperature of interior wall is perceived to be lowest in ft. case, followed by nc case, and the multilayer wall system with cl case has the highest temperature on interior wall. It is found that average temperature of the interior wall increases with elapse of time, reaching maximal results of 30.23, 29.97 and 28.5 °C for the multilayer wall systems containing ft., nc and cl cases at 24 h. Results prove that ft. case has best heat dissipation performance to resolve the building overheating issue. When it comes to average temperature of the exterior wall, Fig. 12(a) indicates that it achieves slight increase owing to thermal resistance of the multilayer wall system.

Heat dissipation rate from building indoor environment is plotted in Fig. 12(b) and it is determined to decrease sharply as the measured time elapses. Since the multilayer wall system is enhanced by ft. and nc cases, the transient heat dissipation rate also reduces in the order of ft., nc and cl cases, revealing the lowest result of approximately 19.275, 11.190 and 9.741 W/m^2 at 24 h. In comparison to indoor temperature of 32 °C, the multilayer wall system with ft. case has preferable capacity to eliminate overheating issue of well insulated buildings. Fig. 12(c) plots the heat dissipation rate varied with time when the indoor temperature decreases from 32 to 24 °C. It is exhibited that reduced temperature difference between indoor and the multilayer wall system induces lower transient heat dissipation rate. Heat dissipation rate from the multilayer wall system drops with the elapse of time and can fall down to merely 11.811 and 5.905 W/m^2 at 24 h under indoor temperature of 28 and 24 °C, respectively.

Heat dissipation rates of the multilayer wall system including DIS-PCM case at the indoor temperature of 24 °C is presented in Fig. 12 (d). It is apparent that transient average heat dissipation rate of the ft.

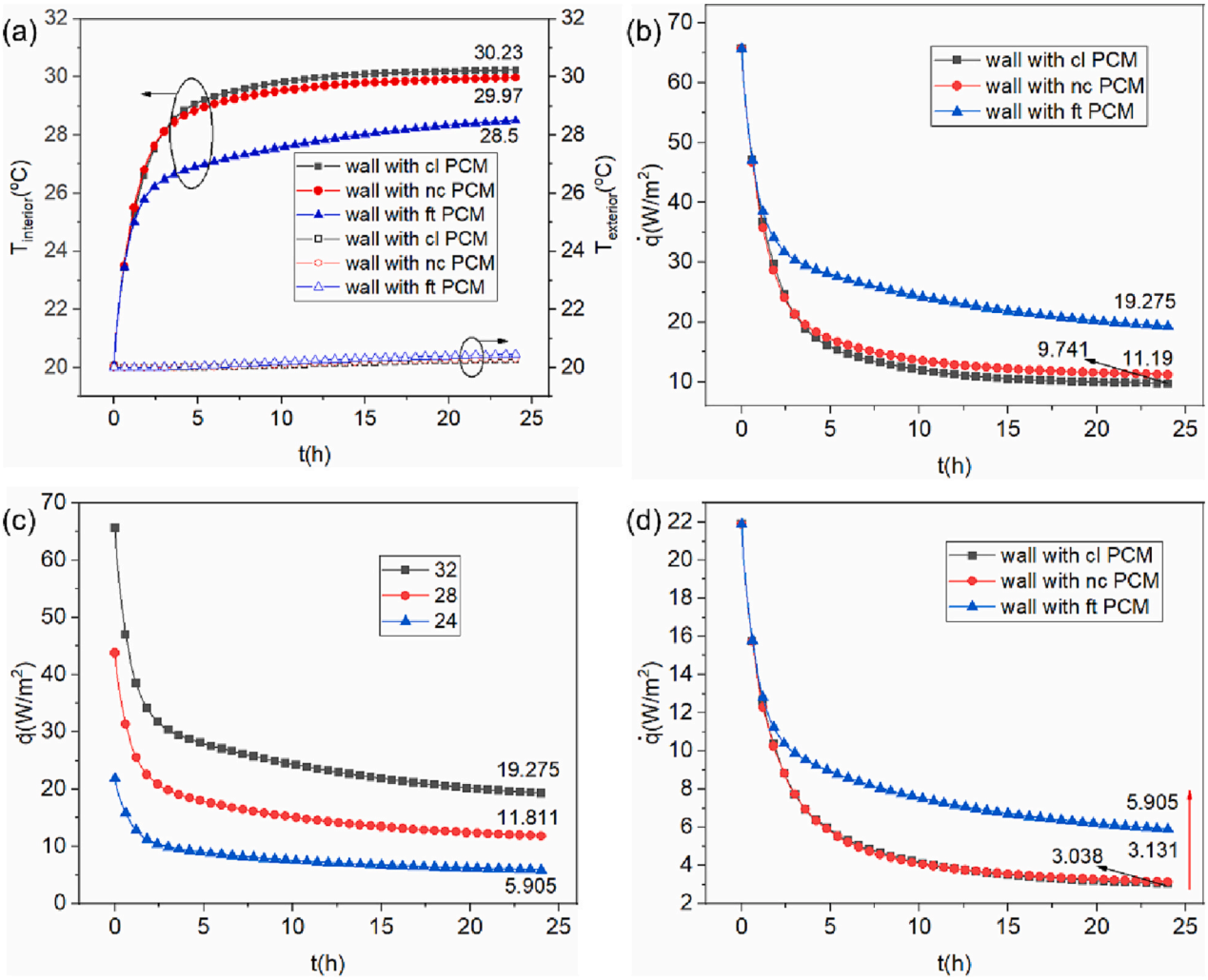

Fig. 12. Performance of the built multilayer wall system at constant ambient temperature. (a) Interior and exterior average temperatures of the multilayer wall (T_{amb} = 20 °C, T_{indoor} = 32 °C); (b) Average heat dissipation rate of the multilayer wall (T_{amb} = 20 °C, T_{indoor} = 32 °C); (c) Average heat dissipation rate of the multilayer wall with ft. case (T_{amb} = 20 °C, T_{indoor} = 32– 24 °C) and (d) Average heat dissipation rate of the multilayer wall (T_{amb} = 20 °C, T_{indoor} = 24 °C).

case based multilayer wall system is much larger than other two cases. Though heat dissipation rate of the multilayer wall system decreases as time continues to elapse, the multilayer wall system having ft. case still has heat dissipation rate of approximately 5.905 W/m^2 which is larger than those of nc and ft. cases (3.131 and 3.038 W/m^2). It is rationally concluded that ft. case is capable of removing excess heat from indoor thermal environment even at less temperature difference between indoor and ambient.

3.3.2. *Variable ambient temperature*

This paper further focuses on thermal performance analysis of the multilayer wall system with ft. case under variable ambient

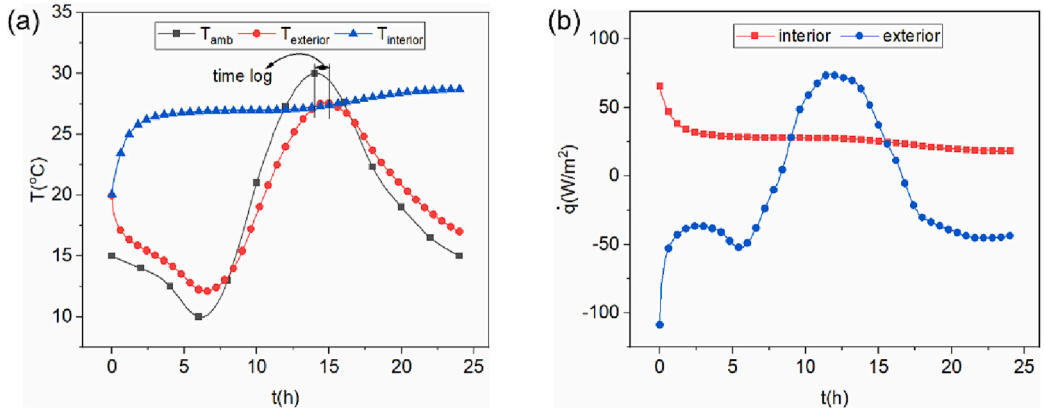

Fig. 13. Performance of the built multilayer wall system with ft. case at variable ambient temperature. (a) Average temperature; (b) Heat dissipation rate.

temperatures of 10 to 30 °C. The indoor temperature is set at 32 °C, meaning the building is suffering from overheating problem. The top and bottom surfaces are termed as adiabatic boundaries. It is apparent in Fig. 13(a) that average temperature on the interior wall increases significantly in the initial stage, as heat is transferred from indoor environment to the multilayer wall system. With elapse of measured time, lower heat exchange rate between indoor and the multilayer wall system brings temperature of the interior wall to increase slowly. It is observed that average temperature of the interior wall fluctuates within a tiny range of 27 to 28.69 °C which creates steady heat dissipation rate from indoor thermal environment and then enables to settle building overheating. Specifically, indoor thermal comfortable temperature can be adjusted according to the air flowing rate. That is to say, larger or lower air flowing rate results in corresponding higher or less indoor temperature. It is demonstrated in Fig. 13(a) that average temperature of the exterior wall displays similar fluctuation to the ambient temperature, due to the direct convective heat transfer between the multilayer wall system and ambient. Thermal inertia of the multilayer wall system also causes a time lag of 0.7 h between average temperature of the exterior wall and ambient temperature.

Heat dissipation rates on interior and exterior walls of the multilayer wall system are evaluated in Fig. 13(b). It is found that they change substantially with elapse of measured time. As the indoor temperature is always higher than ambient temperature, thermal energy can be discharged from indoor thermal environment to ambient. Average temperature of the interior wall gradually increases as the measured time rises, presenting continuous decline of average heat dissipation rate on the interior wall. Average heat dissipation rate on the interior wall then fluctuates between 27.748 and 18.216 W/m^2 over the measured time, which is favorable to relieve building overheating. As to the exterior wall of the multilayer wall system, heat dissipation rate shows noticeable fluctuation under the convective heat transfer between the multilayer wall system and ambient. Heat dissipation rate will be below or above 0 when average temperature of the exterior wall is higher than or lower than ambient temperature. The maximal heat dissipation rate of 74.397 W/m^2 appears at 11.7 h on the exterior wall, as indicated in Fig. 13(b).

4. Conclusions

PCM has the capacity to reduce indoor temperature fluctuation based on its latent heat storage capacity when utilized in building energy conservation. However, the building integrated with PCM produces a large thermal barrier between indoor thermal environment and ambient, usually causing overheating problem occurred in summer. This paper introduces DIS into a PCM system to configure a composite structure with switchable thermal resistance to overcome building overheating issue and improve indoor thermal comfort with less energy consumption. Numerical model is conducted, verified by experimental tests, to analyze phase change heat transfer performance and effective thermal resistance of the DIS-PCM composite system. Effects of H/L ratio and height of PCM cavity, air flowing rate as well as inputted heat flux on the DIS-PCM system are comprehensively evaluated.

It is found that thermal resistance of PCM modules can be significantly modified by natural convection and forced turbulence of air. The ft. case obtains the lowest thermal resistance, orderly followed by nc and cl cases. Average heat dissipation rates of PCM modules increase with argument of time and can approach to 16.119, 28.387 and 34.192 W/m^2 in cl, nc and ft. cases, respectively. Temperature and phase change contour indicate that forced turbulence of air in ft. case enables to promote uniformity of temperature and phase transition distribution. Remarkable temperature variation is only observed in the top regions of cl and nc cases, which is attributed to high-temperature air floating up along the PCM module under the spontaneously thermal buoyancy. Liquid fraction of PCM in three modules remarkably increases as time elapses, individually attaining 0.518, 0.424 and 0.218 at 24 h in cl, nc and ft. cases. Larger H/L ratio of PCM cavity inducing more intensive air flow is conducive to heat transfer between air and PCM. The maximal liquid fraction of PCM climbs to 0.252, 0.218, 0.160 and 0.139 in the cases of H210, H200, H180 and H160, respectively. PCM cavity with large height extends effective heat contacting time to improve heat transfer performance between air and PCM. The heat dissipation rates of H100 ~ H1000 cases are individually calculated as 33.523, 34.192, 32.4 and 30.551 W/m^2 at 24 h. Lower flowing rate or larger inputted heat flux results in faster heat transfer rate and earlier PCM melting in contrast to the PCM module. Heat dissipation rates climb up to 34.073 and 61.462 W/m^2, under the air flowing rate and inputted heat flux of 1.00 m/s and 125 W/m^2. Building performance analysis indicates that thermal performance of the multilayer hollow wall system can be largely improved by DIS-PCM system. Lower average temperature of the interior wall and higher heat dissipation rate from indoor thermal environment are found. Heat dissipation rate of the interior wall can be maintained at a high level of 19.275 W/m^2 at 24 h, declining to approximately 11.811 and 5.905 W/m^2 at indoor temperatures of 28 and 24 °C. Steady heat dissipation rate from indoor thermal environment creates interior wall fluctuating within a tiny range of 27 to 28.69 °C under variable ambient temperatures. Indoor thermal comfortable temperature can be accurately adjusted by the air flowing rate.

In conclusion, this novel DIS-PCM system provides a superior strategy to eliminate building overheating through switching its thermal resistance to response various working scenarios, which is conductive to popularize the latent heat storage applied in building energy conservation.

CRediT authorship contribution statement

Zhaoli Zhang: Conceptualization, Methodology, Writing - Original draft preparation. Nan Zhang: Data curation, Writing - Review & Editing, Supervision. Yanping Yuan: Writing - Review & Editing, Visualization. Patrick E. Phelan: Resources, Writing - Review & Editing, Visualization. Shady Attia: Resources, Writing - Review & Editing, Visualization.

Declaration of competing interest

The authors declare that they have no known competing financial interests or personal relationships that could have appeared to influence the work reported in this paper.

Data availability

Data will be made available on request.

Acknowledgements

This work was supported by the National Natural Science Foundation of China (NO. 52108077 and 52006183), the Natural Science Foundation of Jiangsu Province (NO. BK20190860).

References

[1] I. Andrić, M. Koc, S.G. Al-Ghamdi, A review of climate change implications for built environment: impacts, mitigation measures and associated challenges in developed and developing countries, J. Clean. Prod. 211 (2019) 83–102, https://doi.org/10.1016/j.jclepro.2018.11.128.

[2] Y. Yu, L. Chen, J. Wang, Y. Zhao, J. Song, Implications of power industry marketization for sustainable generation portfolios in China, J. Clean. Prod. (2022), 134541, https://doi.org/10.1016/j.jclepro.2022.134541.

[3] L. Yang, H. Yan, J.C. Lam, Thermal comfort and building energy consumption implications – a review, Appl. Energy 115 (2014) 164–173, https://doi.org/10.1016/j.apenergy.2013.10.062.

[4] H. Zhao, F. Magoulès, A review on the prediction of building energy consumption, Renew. Sust. Energ. Rev. 16 (2012) 3586–3592, https://doi.org/10.1016/j.rser.2012.02.049.

[5] K. Faraj, M. Khaled, J. Faraj, F. Hachem, C. Castelain, A review on phase change materials for thermal energy storage in buildings: heating and hybrid applications, J. Energy Storage 33 (2021), 101913, https://doi.org/10.1016/j.est.2020.101913.
[6] S.R.L. da Cunha, J.L.B. de Aguiar, Phase change materials and energy efficiency of buildings: a review of knowledge, J. Energy Storage 27 (2020), https://doi.org/10.1016/j.est.2019.101083.
[7] R. Zeinelabdein, S. Omer, E. Mohamed, Parametric study of a sustainable cooling system integrating phase change material energy storage for buildings, J. Energy Storage 32 (2020), 101972, https://doi.org/10.1016/j.est.2020.101972.
[8] J. Jia, B. Liu, L. Ma, H. Wang, D. Li, Y. Wang, Energy saving performance optimization and regional adaptability of prefabricated buildings with PCM in different climates, Case Stud. Therm. Eng. 26 (2021), 101164, https://doi.org/10.1016/j.csite.2021.101164.
[9] E. Meng, J. Yang, B. Zhou, C. Wang, J. Li, Preparation and thermal performance of phase change material (PCM) foamed cement used for the roof, J. Build. Eng. 53 (2022), 104579, https://doi.org/10.1016/j.jobe.2022.104579.
[10] Y. Huang, S. Yang, M. Aadmi, Y. Wang, M. Karkri, Z. Zhang, Numerical analysis on phase change progress and thermal performance of different roofs integrated with phase change material (PCM) in moroccan semi-arid and Mediterranean climates, Build. Simul. 16 (2023) 69–85, https://doi.org/10.1007/s12273-022-0922-z.
[11] X. Xie, B. Xu, X. Ni Chen, G. Pei, Turning points emerging in the effect of thermal conductivity of phase change materials on utilization rate of latent heat in buildings, Renew. Energy 179 (2021) 1522–1536, https://doi.org/10.1016/j.renene.2021.07.129.
[12] M. Hagenau, M. Jradi, Dynamic modeling and performance evaluation of building envelope enhanced with phase change material under danish conditions, J. Energy Storage 30 (2020), 101536, https://doi.org/10.1016/j.est.2020.101536.
[13] O.J. Imafidon, D.S.-K. Ting, Energy consumption of a building with phase change material walls – the effect of phase change material properties, J. Energy Storage 52 (2022), 105080, https://doi.org/10.1016/j.est.2022.105080.
[14] M.A. Abdel-Mawla, M.A. Hassan, A. Khalil, Impact of placement and design of phase change materials in thermally activated buildings, J. Energy Storage 56 (2022), 105886, https://doi.org/10.1016/j.est.2022.105886.
[15] R.D. Beltrán, J. Martínez-Gómez, Analysis of phase change materials (PCM) for building wallboards based on the effect of environment, J. Build. Eng. 24 (2019), 100726, https://doi.org/10.1016/j.jobe.2019.02.018.
[16] X. Sun, Y. Lin, Z. Zhu, J. Li, Optimized design of a distributed photovoltaic system in a building with phase change materials, Appl. Energy 306 (2022), 118010, https://doi.org/10.1016/j.apenergy.2021.118010.
[17] S. Alqaed, J. Mustafa, F.A. Almehmadi, The effect of using phase change materials in a solar wall on the number of times of air conditioning per hour during day and night in different thicknesses of the solar wall, J. Build. Eng. 51 (2022), 104227, https://doi.org/10.1016/j.jobe.2022.104227.
[18] T. Long, W. Li, Y. Lv, Y. Li, S. Liu, J. Lu, S. Huang, Y. Zhang, Benefits of integrating phase-change material with solar chimney and earth-to-air heat exchanger system for passive ventilation and cooling in summer, J. Energy Storage 48 (2022), 104037, https://doi.org/10.1016/j.est.2022.104037.
[19] Y. Kharbouch, Effectiveness of phase change material in improving the summer thermal performance of an office building under future climate conditions: an investigation study for the moroccan Mediterranean climate zone, J. Energy Storage. 54 (2022), 105253, https://doi.org/10.1016/j.est.2022.105253.
[20] S. Yang, H. Oliver Gao, F. You, Model predictive control for demand- and market-responsive building energy management by leveraging active latent heat storage, Appl. Energy 327 (2022), 120054, https://doi.org/10.1016/j.apenergy.2022.120054.
[21] M. Vega, N. Llantoy, M. Chafer, S. Ushak, L.F. Cabeza, Life cycle assessment of the inclusion of phase change materials in lightweight buildings, J. Energy Storage. 56 (2022), 105903, https://doi.org/10.1016/j.est.2022.105903.
[22] R.A. Kishore, M.V.A. Bianchi, C. Booten, J. Vidal, R. Jackson, Enhancing building energy performance by effectively using phase change material and dynamic insulation in walls, Appl. Energy 283 (2021), 116306, https://doi.org/10.1016/j.apenergy.2020.116306.
[23] M.S.-E. Imbabi, A passive–active dynamic insulation system for all climates, Int. J. Sustain. Built Environ. 1 (2012) 247–258, https://doi.org/10.1016/j.ijsbe.2013.03.002.
[24] T. Pflug, T.E. Kuhn, R. Nörenberg, A. Glück, N. Nestle, C. Maurer, Closed translucent façade elements with switchable U-value—A novel option for energy management via the facade, Energy Build. 86 (2015) 66–73, https://doi.org/10.1016/j.enbuild.2014.09.082.
[25] T. Pflug, B. Bueno, M. Siroux, T.E. Kuhn, Potential analysis of a new removable insulation system, Energy Build. 154 (2017) 391–403, https://doi.org/10.1016/j.enbuild.2017.08.033.
[26] S.J.M. Koenders, R.C.G.M. Loonen, J.L.M. Hensen, Investigating the potential of a closed-loop dynamic insulation system for opaque building elements, Energy Build. 173 (2018) 409–427, https://doi.org/10.1016/j.enbuild.2018.05.051.
[27] A. Louanate, R. El Otmani, K. Kandoussi, M. Hamed Boutaous, Characterization of the rheological behavior of a paraffin-based phase change material under steady and oscillatory shear, Thermochim. Acta. 704 (2021), 179018, https://doi.org/10.1016/j.tca.2021.179018.
[28] S. Kamali, Review of free cooling system using phase change material for building, Energy Build. 80 (2014) 131–136, https://doi.org/10.1016/j.enbuild.2014.05.021.
[29] W. Zhao, A.F. Elmozughi, A. Oztekin, S. Neti, Heat transfer analysis of encapsulated phase change material for thermal energy storage, Int. J. Heat Mass Transf. 63 (2013) 323–335, https://doi.org/10.1016/j.ijheatmasstransfer.2013.03.061.
[30] J. Woodfield, M. Alvarez, B. Gómez-Vargas, R. Ruiz-Baier, Stability and finite element approximation of phase change models for natural convection in porous media, J. Comput. Appl. Math. 360 (2019) 117–137, https://doi.org/10.1016/j.cam.2019.04.003.
[31] A.D. Brent, V.R. Voller, K.J. Reid, Enthalpy-porosity technique for modeling convection-diffusion phase change: application to the melting of a pure metal, Numer. Heat Transf. 13 (1988) 297–318, https://doi.org/10.1080/10407788808913615.
[32] Z. Younsi, H. Naji, A numerical investigation of melting phase change process via the enthalpy-porosity approach: application to hydrated salts, Int. Commun. Heat Mass Transf. 86 (2017) 12–24, https://doi.org/10.1016/j.icheatmasstransfer.2017.05.012.
[33] A. Padhi, S.K. Dash, Shape effect on natural convection heat transfer over a constant surface area vertical hollow frustum, Int. Commun. Heat Mass Transf. 138 (2022), 106373, https://doi.org/10.1016/j.icheatmasstransfer.2022.106373.
[34] M.K. Dash, S.K. Dash, Natural convection heat transfer and fluid flow around a thick hollow vertical cylinder suspended in air: a numerical approach, Int. J. Therm. Sci. 152 (2020), 106312, https://doi.org/10.1016/j.ijthermalsci.2020.106312.
[35] Y. Xue, X. Li, Z. Wang, H. Wang, Numerical study of modeling methods and evaluation indexes for jet fans, Build. Environ. 206 (2021), 108284, https://doi.org/10.1016/j.buildenv.2021.108284.
[36] J. Tiwari, T. Yeom, Enhancement of channel-flow convection heat transfer using piezoelectric fans, Appl. Therm. Eng. 191 (2021), 116917, https://doi.org/10.1016/j.applthermaleng.2021.116917.